nature COMMUNICATIONS

ARTICLE

Received 21 Feb 2014 | Accepted 27 Aug 2014 | Published 30 Sep 2014

DOI: 10.1038/ncomms6098

Jumonji demethylases moderate precocious flowering at elevated temperature via regulation of *FLC* in *Arabidopsis*

Eng-Seng Gan[1,2], Yifeng Xu[1], Jie-Yun Wong[1], Jessamine Geraldine Goh[1,†], Bo Sun[1], Wan-Yi Wee[1], Jiangbo Huang[1,2] & Toshiro Ito[1,2]

As sessile organisms, plants have evolved multiple mechanisms to respond to environmental changes to improve survival. *Arabidopsis* plants show accelerated flowering at increased temperatures. Here we show that Jumonji-C domain-containing protein JMJ30 directly binds to the flowering-repressor *FLOWERING LOCUS C* (*FLC*) locus and removes the repressive histone modification H3 lysine 27 trimethylation (H3K27me3). At elevated temperatures, the *JMJ30* RNA and protein are stabilized, and *FLC* expression is maintained at high levels to prevent extreme precocious flowering. The double mutant of *JMJ30* and its homologue *JMJ32*, grown at elevated temperatures, exhibits an early-flowering phenotype similar to the *flc* mutant, which is associated with increased H3K27me3 levels at the *FLC* locus and decreased *FLC* expression. Furthermore, ectopic expression of *JMJ30* causes an *FLC*-dependent late-flowering phenotype. Taken together, JMJ30/JMJ32-mediated histone demethylation at the *FLC* locus constitutes a balancing mechanism in flowering control at warm temperatures to prevent premature early flowering.

[1] Temasek Life Sciences Laboratory (TLL), 1 Research Link, National University of Singapore, Singapore 117604, Singapore. [2] Department of Biological Sciences, Faculty of Science, National University of Singapore, 10 Science Drive 4, Singapore 117543, Singapore. † Present address: Division of Infectious Diseases, Department of Medicine, National University Health System (NUHS), 5 Lower Kent Ridge Road, Singapore 119074, Singapore. Correspondence and requests for materials should be addressed to T.I. (email: itot@tll.org.sg).

Unlike animals, plants are sessile organisms that stay in the same location throughout their life cycle and are continually exposed to fluctuating ambient conditions, thus highlighting the importance of rapid adaptation to increase the odds of survival. Plants have evolved a myriad of mechanisms to perceive environmental conditions and respond to these changes, as deviations from normal growth conditions could stress the plants and have severe effects on their growth and development. The inevitable changes to the global climate represent an emerging threat, as many plants are highly sensitive to temperature fluctuations[1]. A slight increase or decrease in ambient temperature could affect the growth rate, organ maturation and function, and flowering transition[2,3].

Under normal growth conditions, upon reaching a certain developmental stage and perceiving the right environmental cues, plants would undergo a floral transition. In *Arabidopsis*, this switch from a vegetative to a reproductive phase is controlled by four pathways, and all inputs congregate on a few key floral regulators: the floral repressor *FLOWERING LOCUS C* (*FLC*), which acts upstream and represses the downstream floral inducers *FLOWERING LOCUS T* (*FT*) and *SUPPRESSOR OF OVEREXPRESSION OF CONSTANS 1* (*SOC1*)[4–7]. In addition, recent findings have revealed a few players involved in a fifth flowering pathway that is responsive to ambient temperature changes and has been called the thermosensory pathway. Elevated ambient temperatures accelerate flowering by reducing the repressive H2A.Z nucleosome occupancy at the *FT* locus, which then allows the transcription factor PHYTOCHROME INTERACTING FACTOR 4 (PIF4) to bind and activate *FT*[8,9]. On the other hand, the MADS-box heterocomplex containing SHORT VEGETATIVE PHASE (SVP) and a temperature-dependent isoform of FLOWERING LOCUS M (FLM) represses flowering at lower temperatures[10–14]. The floral repressor *FLC* was also shown to delay flowering during short exposures to non-freezing cold temperatures[15]. These findings suggest the interplay of multiple thermosensory mechanisms in controlling flowering in response to ambient temperature fluctuations.

Considering how the important 'decision' of the vegetative-reproductive phase change centres on just a few genes, it is not surprising that in addition to regulation by transcription factors, many chromatin remodelling mechanisms have evolved to tightly control the expression of these genes. Accelerated flowering by vernalization treatment involves the epigenetic silencing of *FLC* through the Polycomb Group (PcG)-mediated gradual deposition of the trimethylation of lysine 27 of histone H3 (H3K27me3)[16]. Even when plants are grown under normal non-vernalized conditions, the PRC2-like complex containing CURLY LEAF, EMBRYONIC FLOWER 2 and FERTILIZATION-INDEPENDENT ENDOSPERM represses *FLC* expression during vegetative development[17]. In addition to H3K27me3, *FLC* expression is also regulated by repressive H3K9me2 marks, activating H3K4me3/H3K36me3 marks, and histone acetylation[5,18,19]. These crosstalks of histone marks at the locus depend on the interplay between histone methyltransferases and histone demethylases[20,21].

There are two known classes of histone demethylases, and only the Jumonji-C (JmjC) domain-containing proteins have the ability to demethylate trimethylated histones. There are 21 *JUMONJI* (*JMJ*) genes in *Arabidopsis*, which can be categorized into five groups, namely the KDM5/JARID1, KDM4/JHDM3/JMJD2, KDM3/JHDM2, JMJD6 and JmjC domain-only group, based on their JmjC domain sequences and domain architectures[22,23]. Members from the same group show similar target specificity for histone modifications[24–32]. One of the histone modifications, the repressive PcG-mediated H3K27me3, plays a key role in gene repression and developmental regulation, and is actively and dynamically deposited and removed in plants[33]. However, although the demethylases for H3K27me3, UTX and JMJD3 were found years ago in animals[34], there is no *Arabidopsis* homologue in the same KDM6/JMJD3 group. Only recently, members from the KDM4/JHDM3/JMJD2 group, RELATIVE OF EARLY FLOWERING 6 (REF6) in *Arabidopsis* and JMJ705 in rice, were reported as H3K27me3 demethylases[29,35].

Early flowering at high temperatures mediated by the thermosensory pathways is considered to be an adaptive trait to maximize the reproductive success. However, flowering too early without sufficient vegetative growth may risk not having enough nutrients and resources to support seed maturation. Here we show that JMJ30/AT3G20810 and JMJ32/AT3G45880, two members of the JmjC domain-only group of JMJ proteins, function as H3K27 demethylases and regulate *FLC* expression in *Arabidopsis*. Our results suggest that JMJ30/JMJ32-mediated *FLC* regulation may constitute a balancing mechanism that controls flowering time to ensure reproductive success at elevated temperatures.

Results

***FLC* prevents precocious flowering at elevated temperatures.** The flowering time of the *flc-3* null mutant is indistinguishable from Columbia wild-type (WT) plants when grown at 22 °C under long day (LD, 16-h light/8-h dark) conditions (Fig. 1a,b)[36,37]. However, when grown at 29 °C LD conditions, *flc-3* plants flowered earlier than WT plants with the leaf number ratio (29 °C/22 °C) of 0.51 for *flc-3* and 0.69 for WT (Fig. 1a,b), suggesting that *FLC* contributes to preventing precocious flowering at elevated temperatures[38]. Although *FLC* expression is low in WT plants that lack a functional *FRIGIDA* (*FRI*)[38], expression analyses are still able to detect basal *FLC* expression, which gradually decreases during vegetative development (Fig. 1c)[27]. To determine whether *FLC* temporal expression level is affected by elevated temperatures, we analysed *FLC* expression in plants grown at 22 °C and 29 °C under LD conditions at 5, 9 and 13 days-after-germination (DAG) before the plants undergo the bolting process. We observed that after shifting to 29 °C at 3 DAG, *FLC* expression was initially comparable between plants grown at 22 °C and 29 °C at 5 DAG (Fig. 1c). *FLC* expression decreases gradually at 9 and 13 DAG in plants grown under both the 22 °C and 29 °C conditions, but this *FLC* downregulation is significantly attenuated in plants grown at 29 °C (Fig. 1c). This result showed that *FLC* repression during vegetative development is delayed during growth at elevated temperatures.

We wondered whether this delayed repression is regulated at the chromatin level. As *FLC* reduction during the developmental switch from vegetative to reproductive phase is known to be regulated by the repressive H3K27me3 (refs 16,17), we performed chromatin immunoprecipitation (ChIP) assays to assess the level of H3K27me3 at the *FLC* locus at 8 DAG, which is on the brink of floral transition occurring at 9 DAG[39] (Fig. 1d,e). Compared with WT plants grown under 22 °C LD conditions, WT plants grown at 29 °C showed reduced H3K27me3 enrichment at the *FLC* locus (Fig. 1e). This finding indicates that delayed *FLC* repression at elevated temperatures is associated with the reduction of the repressive H3K27me3 at the *FLC* locus. Taken together, these results suggest that H3K27me3-associated histone modifiers may participate in the thermosensory pathway by regulating *FLC* expression at elevated temperatures to control flowering in moderation.

Mutation of *jmj30* and *jmj32* promotes flowering at 29 °C. The lower levels of H3K27me3 at the *FLC* locus at elevated

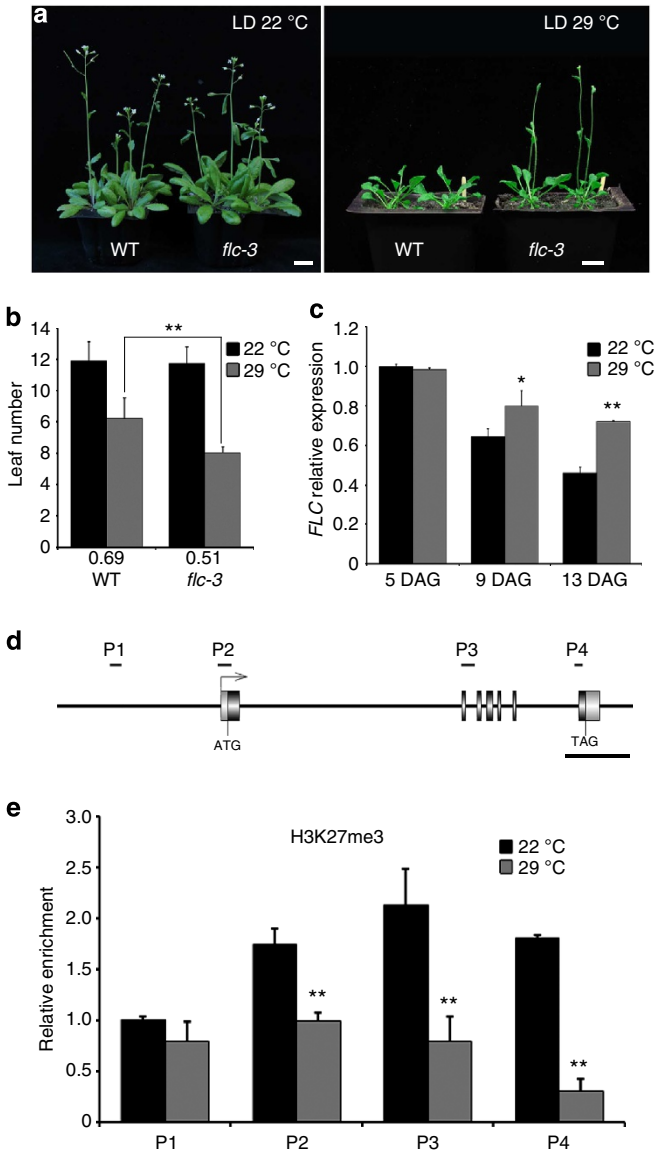

Figure 1 | *FLC* is a suppressor of thermal induction of flowering. (**a**) *flc-3* flowers at a similar time as WT when grown in LD 22 °C, but flowering is accelerated in *flc-3* when grown under LD 29 °C conditions. Representative 30-day-old plants (LD 22 °C) or 23-day-old plants (LD 29 °C) are shown for comparison. Scale bar, 1 cm. (**b**) Total primary rosette leaves before bolting in WT and *flc-3* plants grown under LD 22 °C and 29 °C conditions were counted (two independent experiments with 15–20 plants each). Numbers below graph indicate leaf number ratio (29 °C/22 °C). Bars indicate standard deviation (s.d.); two-tailed Student's *t*-test, $^{**}P<0.01$. (**c**) *FLC* mRNA levels in 5, 9 and 13 DAG seedlings grown under LD 22 °C and 29 °C conditions. Relative fold changes to 5 DAG seedlings grown under 22 °C conditions are presented. Bars indicate s.d. of three biological replicates; two-tailed Student's *t*-test, $^{*}P<0.05$, $^{**}P<0.01$. (**d**) Schematic drawing of the *FLC* genome structure showing regions amplified by primers used for ChIP analysis. Scale bar, 1 kb. (**e**) ChIP analysis of H3K27me3 enrichment at the *FLC* locus in 8 DAG WT seedlings grown under LD 22 °C and 29 °C conditions. An anti-H3 antibody was used as a control. Bar indicates standard error of the mean (s.e.m.) of three biological replicates; two-tailed Student's *t*-test, $^{**}P<0.01$.

temperatures and the increased level of *FLC* expression led us to conjecture that the effect may be maintained through the action of H3K27me3 demethylases. However, *FLC* expression is upregulated rather than downregulated in the loss-of-function mutant of the only known *Arabidopsis* H3K27me3 demethylase, *REF6* (refs 29,40). Hence, we reasoned that there might be other JMJ proteins that may remove the H3K27me3 repressive marks at the *FLC* locus.

Among the five groups of *Arabidopsis* JMJ proteins, four of them (KDM5/JARID1, KDM4/JHDM3/JMJD2, KDM3/JHDM2 and JMJD6) have been implicated as histone demethylases specific for other histone modifications, such as H3K4 and H3K9 (refs 22–32). Little is known about the enzymatic function of the JmjC domain-only group that contains no other known functional protein domains but the catalytic JmjC domain, except their role in circadian regulation[41,42]. To elucidate the function of this group, we used two previously described loss-of-function mutants for *JMJ30*: *jmj30-1* (SAIL_811_H12) and *jmj30-2* (GK-454C10)[41,42], and isolated one T-DNA insertional mutant for *JMJ32*: *jmj32-1* (SALK_003313; Fig. 2a). No full-length *JMJ30* mRNA was detected for either allele, and we decided to use *jmj30-2* for subsequent experiments, as it produced no partial fragments (Fig. 2b, Supplementary Fig. 1a,b). No full-length *JMJ32* mRNA was detected in *jmj32-1*, but partial fragments were still detectable (Fig. 2b, Supplementary Fig. 1a,c). However, because the T-DNA is inserted at the catalytic JmjC domain in *jmj32-1* (Fig. 2a), it likely produces a null mutant. Under the standard growth conditions (22 °C LD), neither the single nor the double *jmj30-2 jmj32-1* (herein *jmj30 jmj32*) mutants differed from WT in terms of flowering time, which is similar to the *flc* mutant's lack of a phenotype under standard growth conditions (Figs 1a,b and 2c,d). However, we found that the *jmj30 jmj32* double mutant flowered earlier than the WT when grown under elevated temperatures with the decreased leaf number ratio (29 °C/22 °C) of 0.52 compared with 0.69 in WT, but no obvious difference in phyllochron length (Fig. 2c,d), as was observed in *flc* (Fig. 1a,b). We then studied the response of *jmj30 jmj32* to elevated temperature in short days (SDs, 8-h light/16-h dark) and observed the enhanced early-flowering phenotype compared with WT grown under the same conditions, with the leaf number ratio (29 °C/22 °C) of 0.19 for *jmj30 jmj32* and 0.24 for WT (Supplementary Fig. 2a,b).

We next proceed to look at the expression profile of the flowering time genes. We collected 5, 9 and 13 DAG seedling samples grown at 29 °C LD conditions at the end of the light photoperiod. The *jmj30 jmj32* double mutant decreased *FLC* expression at all tested time points (Fig. 3a). Furthermore, the trend of decreased *FLC* expression at 13 DAG is similar in *jmj30 jmj32* seedlings grown at 29 °C (Fig. 3a) and WT grown at 22 °C (Fig. 1c). The other thermosensory mediator *SVP* was not significantly affected (Fig. 3b). In contrast, the expression of the florigen *FT* and another floral promoter *SOC1* were increased especially in 13 DAG seedlings of *jmj30 jmj32* relative to WT at 29 °C LD (Fig. 3c,d). These results align with reports that the FLC-SVP complex represses *FT* in leaves and *SOC1* in both leaves and shoot apical meristems[43]. *AGAMOUS-LIKE 24* (*AGL24*) and *CONSTANS* (*CO*) were not significantly affected in *jmj30 jmj32* (Fig. 3e,f). In short, the results suggest that *jmj30 jmj32* mutations decrease *FLC* expression at elevated temperatures, and this effect appears to upregulate the floral integrators *FT* and *SOC1*, which are two common targets of FLC.

Characterization of JMJ30 and JMJ32. To further reveal the function of JMJ30 and JMJ32, we characterized their spatial expression patterns. Transcript profiling data deposited at the *Arabidopsis* eFP Browser suggest that *JMJ30* and *JMJ32* are rather ubiquitously expressed at the rosette leaves, shoot apex and developing flowers (Supplementary Fig. 3a,b)[44]. To confirm this,

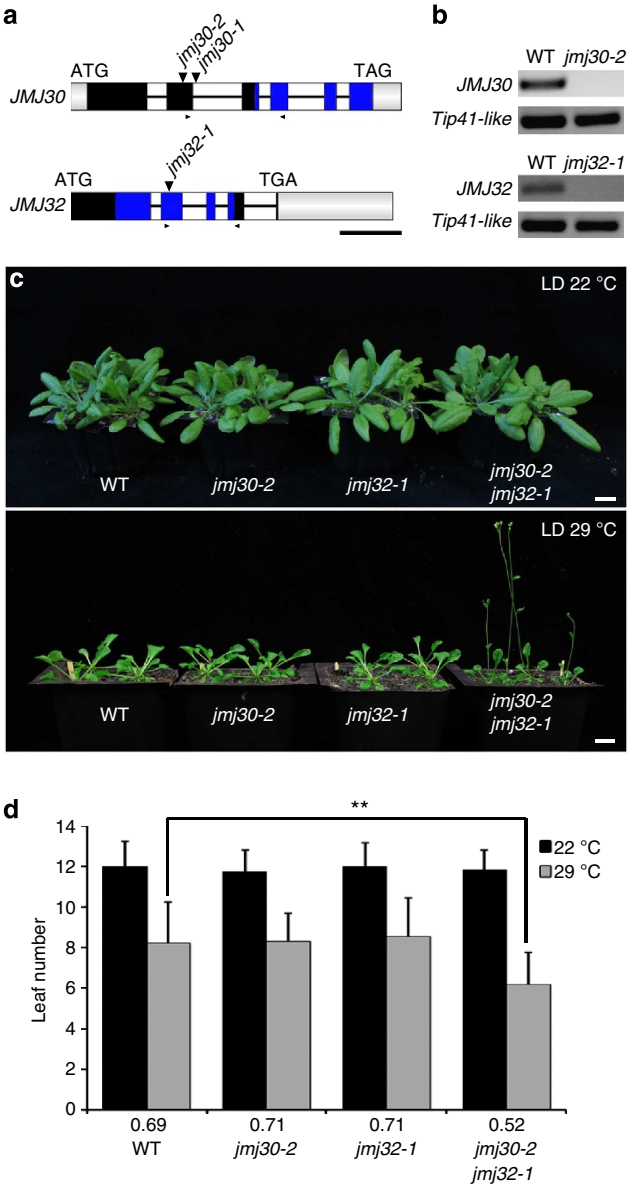

Figure 2 | *jmj30 jmj32* loss-of-function mutant accelerates flowering at elevated temperatures. (**a**) Schematic drawings of *JMJ30* and *JMJ32* genomic structures. Grey boxes indicate the 5′and 3′ untranslated region (UTR). Black boxes indicate exons, whereas blue boxes indicate exons coding for the JmjC domain. White boxes with a line indicate introns. T-DNA insertion sites are marked by downward pointing arrowheads above the schematic diagrams, whereas smaller arrowheads show primers used for RT–PCR. Scale bar, 500 bp. (**b**) RT–PCR of *JMJ30* and *JMJ32* in WT, *jmj30-2* and *jmj32-1*. *Tip-41 like* is shown as an internal control. (**c**) *jmj30-2*, *jmj32-1* and *jmj30-2 jmj32-1* flower at a similar time as WT when grown under LD 22 °C conditions, but *jmj30-2 jmj32-1* showed accelerated flowering when grown under LD 29 °C conditions. Representative 25-day-old plants (LD 22 °C) or 23-day-old plants (LD 29 °C) were shown as comparison. Scale bar, 1 cm. (**d**) Total primary rosette leaves before bolting in WT, *jmj30-2*, *jmj32-1* and *jmj30-2 jmj32-1* plants grown under LD 22 °C and 29 °C conditions were counted (two independent experiments with 15–20 plants each). Numbers below graph indicate leaf number ratio (29 °C/22 °C). Bars indicate s.d.; two-tailed Student's *t*-test, $^{**}P<0.01$.

we extracted RNA from different tissues of WT plants, and by reverse transcription–PCR (RT–PCR), we concluded that *JMJ30* and *JMJ32* were expressed in all tested tissue types, namely, seedlings, roots, rosette leaves, cauline leaves, stems and inflorescences (Supplementary Fig. 4a)[22]. *JMJ30* was highly expressed in leaves, whereas *JMJ32* expression showed no appreciable difference across the various tissue types.

Next, to better understand the spatial distribution of JMJ30 and JMJ32 at the protein level, constructs harbouring their upstream promoter and downstream sequences plus the genomic coding sequence (6.1-kb JMJ30 and 5.3-kb JMJ32) fused with the β-glucuronidase (GUS) reporter gene were transformed into WT plants (Fig. 4a). This genomic fragment of JMJ30, when fused with the short haemagglutinin (HA) epitope tag, was sufficient to rescue the *jmj30 jmj32* early-flowering phenotype at 29 °C LD (Supplementary Fig. 5a,b), indicating that the fragment contains all the *cis*-elements necessary to capture the endogenous expression pattern. Histochemical GUS staining results showed that JMJ proteins were rather ubiquitously expressed, including in the leaves, roots and inflorescences (Fig. 4b,c). Furthermore, JMJ30 and JMJ32 expression in the vasculature of leaves overlapped with the expression patterns of their putative targets *FLC*[45], *FT*[46] and *SOC1* (refs 47,48), and FLC is known to directly repress *FT* and *SOC1* in the leaf veins[43].

To study the sub-cellular localization of JMJ30 and JMJ32, we transiently overexpressed JMJ-VENUS in tobacco *Nicotiana benthamiana*. We observed that JMJ30 and JMJ32 localized not only to the nucleus but also occasionally to the endoplasmic reticulum and cytoplasm (Supplementary Fig. 4b) as reported previously[41], which could be artefacts from the overexpression of the JMJ proteins. We thus generated an endogenous *pJMJ30* promoter-driven JMJ30-HA in *jmj30-2,* which complements the early-flowering phenotype of *jmj30 jmj32* (Supplementary Fig. 5a,b), and performed an immunolocalization assay using anti-HA and anti-H3K27me3 antibodies on its protoplasts. We observed that JMJ30-HA localized primarily to the nucleus, consistent with its role as a histone demethylase, and its expression pattern resembled that of H3K27me3 (Fig. 4d,e). Moreover, immunolocalization assay performed using the extracted nuclei from *jmj30-2 pJMJ30::JMJ30-HA* showed that JMJ30-HA localization to the euchromatin but not to the 4′,6-diamidino-2-phenylindole (DAPI)-dense heterochromatic chromocentres, resembling reported localization of H3K27me3 (refs 49,50), and this localization was not affected by the ambient temperature (Supplementary Fig. 4c).

JMJ30 and JMJ32 specifically demethylate H3K27me2/3. Proteins that have the catalytic JmjC domain are known to be histone demethylases[51], and JMJ30-HA localization that resembled the euchromatic histone marks inspired us to study the biochemical function of these histone demethylases. We first determined whether they could demethylate methylated histones *in vitro*. We transiently overexpressed *35S::JMJ30-HA* in tobacco leaves and immunoaffinity-purified the protein using anti-HA agarose beads. Using these purified proteins, an *in vitro* demethylase assay was carried out. We incubated calf thymus histones with JMJ30-HA proteins, together with reported JmjC cofactors Fe(II) ions and α-ketoglutarate (α-KG). Indeed, western blotting analyses indicated that JMJ30-HA was able to demethylate oligonucleosomes at H3K27me3 and H3K27me2 but not at H3K27me1 (Fig. 5a).

To investigate the demethylase activity of JMJ30 further, we purified a mutated version of JMJ30-HA (JMJ30H326A-HA), in which one of its conserved Fe(II)-binding histidine residues in the JmjC domain was mutated to alanine. We found that the effect of JMJ30H326A-HA on H3K27me2/3 was completely abolished by the mutation (Fig. 5b). To address their substrate specificity, we looked at their ability to demethylate other histone methylation

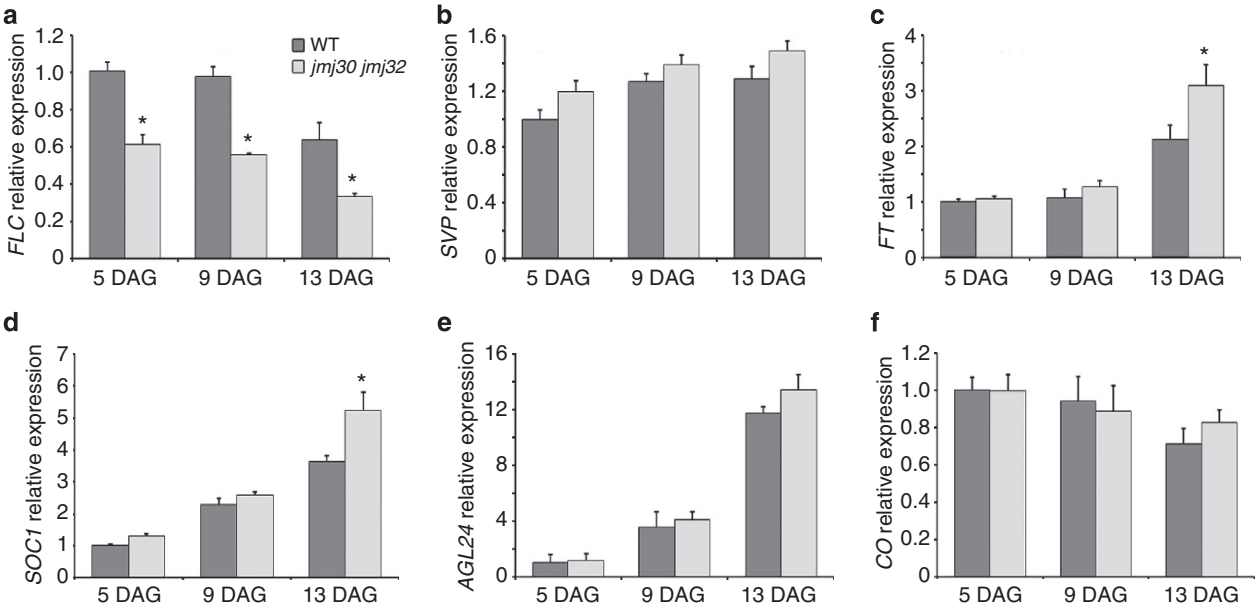

Figure 3 | Expression profiles of flowering time genes. (**a**–**f**) RT–qPCR-based expression profiles of (**a**) *FLC*, (**b**) *SVP*, (**c**) *FT*, (**d**) *SOC1*, (**e**) *AGL24* and (**f**) *CO* in 5, 9 and 13 DAG seedlings of WT and *jmj30-2 jmj32-1* grown under LD 29 °C conditions. Relative fold changes to WT 5 DAG seedlings are presented. Bars indicate s.d. of three biological replicates; two-tailed Student's *t*-test, $^{*}P<0.05$.

marks. Consistent with the previously reported group-specific characteristics of JMJ proteins, we did not see noticeable demethylation activity for H3K4me2/3, H3K9me2/3 and H3K36me2/3 in the *in vitro* demethylase assay (Fig. 5a). The results indicate that JMJ30 can specifically demethylate H3K27me2/3 *in vitro* and that its activity is dependent on its JmjC domain.

Next, to confirm whether JMJ30 and JMJ32 can exert this demethylase activity in plants, we transiently overexpressed *35S::JMJ30-HA* and *35S::JMJ32-HA*, and their respective mutated versions of *35S::JMJ30H326A-HA* and *35S::JMJ32H174A-HA* in *Arabidopsis* leaf protoplasts. Immunostaining assays were then conducted on the isolated nuclei using anti-H3K27me3 and anti-HA antibodies to observe their demethylase activity *in vivo*. We found that the overexpression of JMJ30-HA reduced H3K27me3 levels, however, overexpression of the mutated JMJ30H326A-HA has no effect on H3K27me3 methylation (Supplementary Fig. 6a,b). Similarly, the H3K27me3 levels were reduced in nuclei overexpressing JMJ32-HA but not in the mutated JMJ32H174A-HA-expressing nuclei (Supplementary Fig. 6c,d). Taken together, these results indicate that JMJ30 and JMJ32 function as H3K27me3 demethylases.

***JMJ30* overexpression delays flowering by upregulating *FLC*.** To further elucidate the function of JMJ30, we overexpressed JMJ30-HA in WT plants and confirmed that *35S::JMJ30-HA* transgenic lines exhibit constitutive overexpression of JMJ30 and late-flowering phenotypes at 22 °C LD conditions (Supplementary Fig. 7a–d)[41]. To understand the effects of JMJ30 overexpression at a molecular level, we checked the expression profiles of the flowering time genes in two independent transgenic lines grown at 22 °C under inductive LD conditions. Supporting the phenotypic observations, the floral repressor *FLC* is strongly increased in the *35S::JMJ30-HA* overexpression lines (Fig. 6a). We also found that *FT* and *SOC1* are mildly downregulated (Fig. 6a). As FLC is the common repressor of the two floral integrators[43] and was most significantly affected, the increase in *FLC* expression is likely to be the main reason for the late-flowering phenotype.

Based on the results, we hypothesized that *FLC* is a target of JMJ30. To test whether *FLC* is genetically necessary for JMJ30 functions, we performed a genetic analysis by crossing *35S::JMJ30-HA* with *flc-3*. Introduction of the *flc* mutation largely abolished the late-flowering phenotype of *35S::JMJ30-HA*, and *35S::JMJ30-HA flc-3* flowered at a similar time as *flc-3* or WT plants (Fig. 6b,c). Taken together, these results support the notion that *JMJ30* and *FLC* function in the same genetic pathway that regulates flowering time and that FLC functions downstream of the histone demethylase JMJ30.

JMJ30 and JMJ32 regulate H3K27me3 at the *FLC* locus. Our results suggested that JMJ30 functions as an H3K27me2/3 demethylase *in vitro* (Fig. 5a,b) and *in vivo* (Supplementary Fig. 6a,b), and that *FLC* may be a direct target of JMJ30 (Figs 3a and 6a–c). We were interested in verifying whether the increased *FLC* expression in *JMJ30* overexpression lines is similarly reflected in the H3K27 methylation status of the *FLC* locus. ChIP assays were carried out comparing the H3K27me3 levels between WT and our *35S::JMJ30-HA* plants, and we found that the repressive H3K27me3 levels were decreased at the *FLC* locus in the *35S::JMJ30-HA* lines (Fig. 7a), which is consistent with the increased *FLC* expression levels (Fig. 6a).

We next measured H3K27me3 enrichment at the *FLC* locus in *jmj30 jmj32* and WT grown under 29 °C LD conditions, in which the *jmj30 jmj32* double mutant showed decreased *FLC* expression and accelerated flowering (Figs 2c,d and 3a). Consistent with its expression, we found that the H3K27me3 levels at the *FLC* locus are increased in *jmj30 jmj32* at 29 °C (Fig. 7b). Taken together, these results indicate that JMJ30 and JMJ32 demethylate H3K27me3 at the *FLC* locus to activate *FLC* expression at elevated temperatures.

Prolonged JMJ30 activity directly regulates *FLC* expression. The ability of JMJ30 to affect the H3K27me3 level on *FLC* chromatin leads us to speculate that JMJ30 may directly bind to the *FLC* locus and demethylate the repressive mark. ChIP assays were conducted using the overexpression *35S::JMJ30-HA*

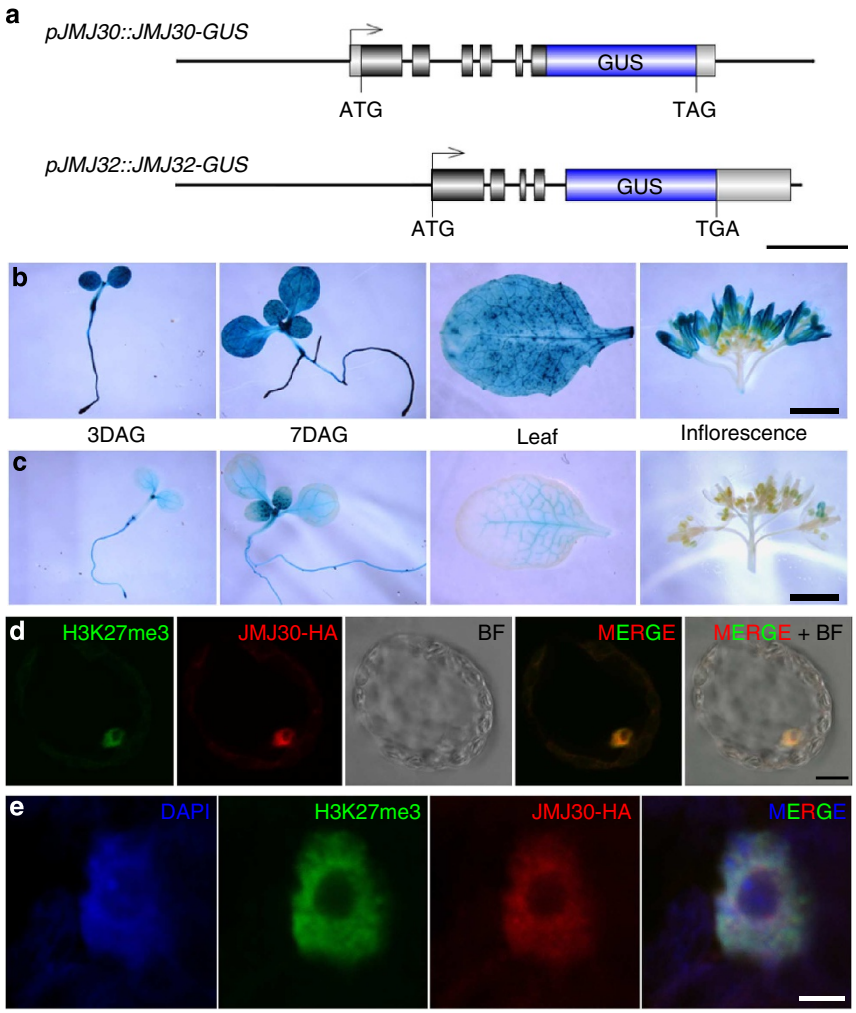

Figure 4 | Spatial expression patterns of JMJ30 and JMJ32. (**a**) Schematic drawings of *pJMJ30::JMJ30-GUS* and *pJMJ32::JMJ32-GUS*. Exons are represented by black boxes, and GUS is represented by blue boxes. Lines indicate promoter, introns and 3′ downstream regions. Scale bar, 1 kb. (**b**,**c**) Histochemical GUS staining of (**b**) *pJMJ30::JMJ30-GUS* and (**c**) *pJMJ32::JMJ32-GUS* transgenic lines. 3 and 7 DAG seedlings, rosette leaves and inflorescences were stained overnight. Scale bars, 2 mm. (**d**,**e**) Immunolocalization of H3K27me3 and JMJ30-HA in protoplasts generated from *jmj30-2 pJMJ30::JMJ30-HA* transgenic lines. (**d**) JMJ30-HA localization resembles that of H3K27me3 in the nucleus. Scale bar, 10 μm. (**e**) Image shows enlarged view of a nucleus. Scale bar, 2.5 μm.

transgenic line and the endogenous promoter-driven *pJMJ30::JMJ30-HA jmj30-2* line grown at 29 °C under LD conditions. We immunoprecipitated the epitope-tagged JMJ30-HA protein using anti-HA agarose to assess the level of JMJ30-HA binding across the *FLC* chromatin region. Compared with WT plants, we found that JMJ30-HA associates with *FLC* chromatin directly in both lines, with the P2 region near the transcriptional start site showing the highest levels of binding enrichment (Fig. 8a; Supplementary Fig. 8).

To further elucidate the mechanism underlying the positive regulation of *FLC* expression at elevated temperatures by JMJ30, we were interested in *JMJ30* mRNA and protein expression and stability at 22 °C and 29 °C. *JMJ30* mRNA diurnal expression has been previously reported[41,42]. Taking samples from WT seedlings grown at 22 °C and 29 °C under LD condition every 4 h, we found that *JMJ30* expression peaked approximately 4 h before dark for both conditions, and the peak levels in the *JMJ30* diurnal expression were not significantly affected by the temperature. However, we found that the width of the peak broadened under the 29 °C conditions (Fig. 8b), which could be due to prolonged expression or increased mRNA stability.

To test if the protein expression of JMJ30 is similarly affected, we did a western blot with total proteins extracted from *jmj30-2 pJMJ30::JMJ30-HA* using an anti-HA-HRP antibody. Under standard growth conditions (22 °C LD), the peak of the JMJ30-HA protein accumulation at the beginning of dark was slightly delayed compared with its mRNA expression, and JMJ30-HA was degraded quickly after that (Fig. 8c). At 29 °C, not only was the JMJ30-HA protein accumulation lengthened, it was also more stable as it persisted much longer than expected based on mRNA expression (Fig. 8b,c). To confirm this, we performed a protein stability assay by pre-treating the seedlings with cycloheximide to prevent *de novo* protein synthesis, and adding the proteasome inhibitor MG132 at the end of the light photoperiod. We collected the samples at different time points and found that the rapid degradation of JMJ30-HA at 22 °C was inhibited by the addition of the proteasome inhibitor MG132 (Supplementary Fig. 9), suggesting that the proteasome-dependent JMJ30-HA degradation is impaired at higher temperatures. These results suggested that the strongly prolonged JMJ30 expression at elevated temperatures may allow JMJ30 to bind and demethylate

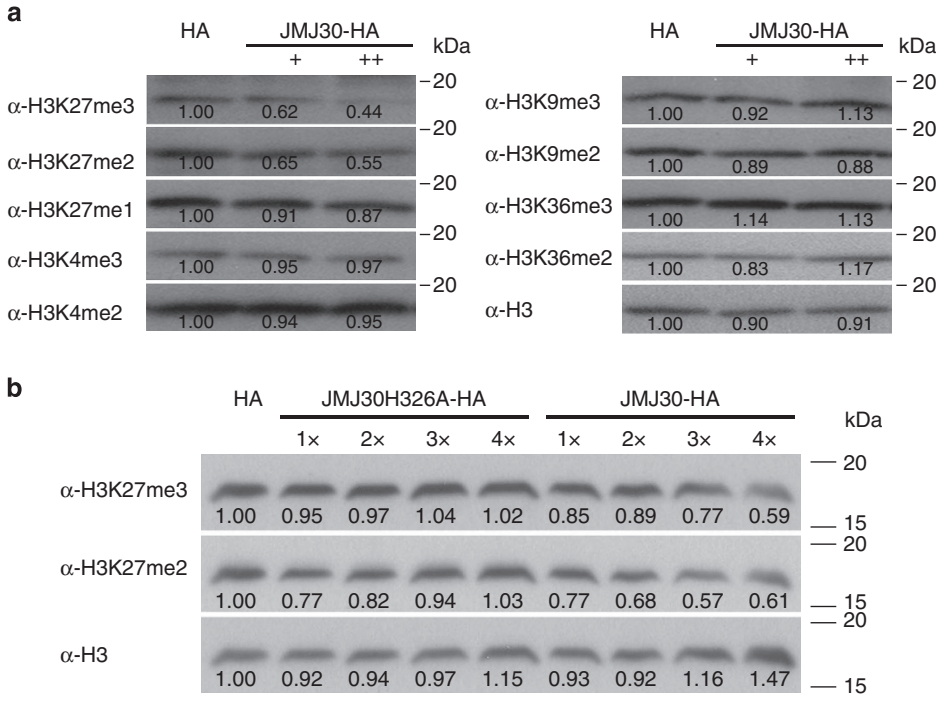

Figure 5 | JMJ30 demethylates H3K27me2/3 *in vitro*. (**a**) Immunoaffinity-purified JMJ30-HA was co-incubated with substrate calf thymus histone and cofactors Fe(II) ions and α-KG at 37 °C for 4 h. Immunoblot analysis of histone demethylase activity of JMJ30 was performed using antibodies indicated to the left. The anti-H3 antibody is used as loading control. (**b**) A mutated version of JMJ30-HA (JMJ30H326A-HA) was unable to demethylate H3K27me2/3 *in vitro* when a conserved Fe(II)-binding histidine residue in the JmjC domain was replaced by alanine. Numbers indicate relative band intensity compared with control reaction (HA) performed using an anti-HA precipitate from WT. At least two biological replicates were performed and one set of the data is shown here.

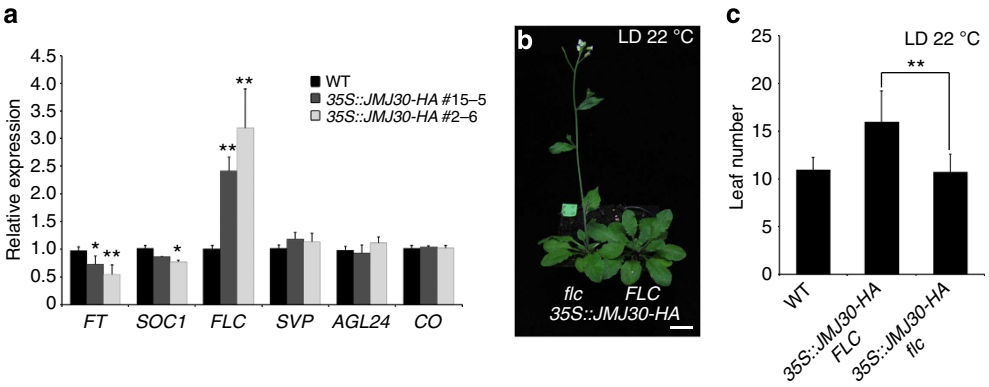

Figure 6 | Overexpression of JMJ30 leads to delayed flowering. (**a**) mRNA expression levels of flowering time genes in WT and two independent lines of *35S::JMJ30-HA*. Relative fold changes to WT are presented. Bars indicate s.d. of three biological replicates; two-tailed Student's *t*-test, $*P<0.05$, $**P<0.01$. (**b**) Introduction of *flc* mutation rescues the late-flowering phenotype of *35S::JMJ30-HA*. Scale bar, 1 cm. (**c**) Total primary rosette leaves before bolting in WT, *35S::JMJ30-HA* and *35S::JMJ30-HA flc* plants grown under LD 22 °C conditions were counted (two independent experiments with 20–50 plants each). Bars indicate s.d.; two-tailed Student's *t*-test, $**P<0.01$.

H3K27me3 at the *FLC* locus, thus maintaining a transcriptionally permissive chromatin status.

JMJ30-regulated genes are enriched for H3K27me3 targets. To investigate whether *JMJ30* overexpression and *jmj30 jmj32* loss-of-function mutants influence gene transcription at a global level, we performed expression profiling using NimbleGen 12 × 135K arrays. Compared with WT, 469 genes were downregulated and 657 genes were upregulated in *jmj30 jmj32* under 29 °C LD conditions (Supplementary Data 1, NCBI Gene Expression Omnibus GSE51898). On the other hand, 516 genes were upregulated and 588 genes were downregulated in *35S::JMJ30-HA* compared with WT (Supplementary Data 2). The transcriptome analyses suggested that despite only showing flowering phenotypes, the loss-of-function and overexpression of *JMJ30* did affect global expression profiles.

Previous studies identified that at least 25% (27.70% of genes analysed in our microarray) of the *Arabidopsis* genome is targeted by H3K27me3 (refs 33,52), and our study showed that JMJ30 and

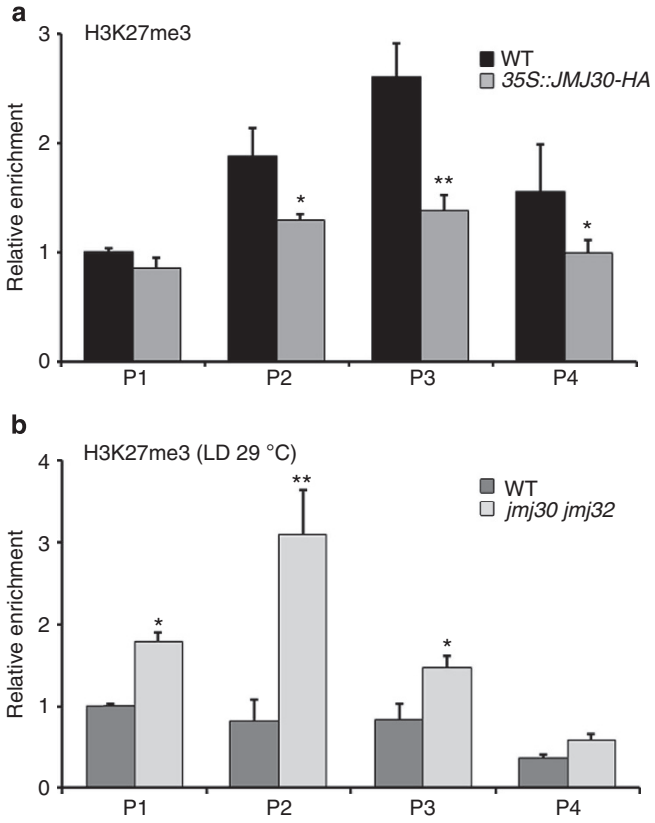

Figure 7 | The repressive H3K27me3 on the *FLC* locus is affected by JMJ30 and JMJ32. (**a**,**b**) ChIP analysis of H3K27me3 enrichment on the *FLC* locus in (**a**) 8 DAG WT and *35S::JMJ30-HA* seedlings grown under LD 22 °C conditions and (**b**) 8 DAG WT and *jmj30 jmj32* seedlings grown under LD 29 °C conditions. An anti-H3 antibody was used as a control. Bar indicates s.e.m. of three biological replicates; two-tailed Student's *t*-test, $*P<0.05$, $**P<0.01$.

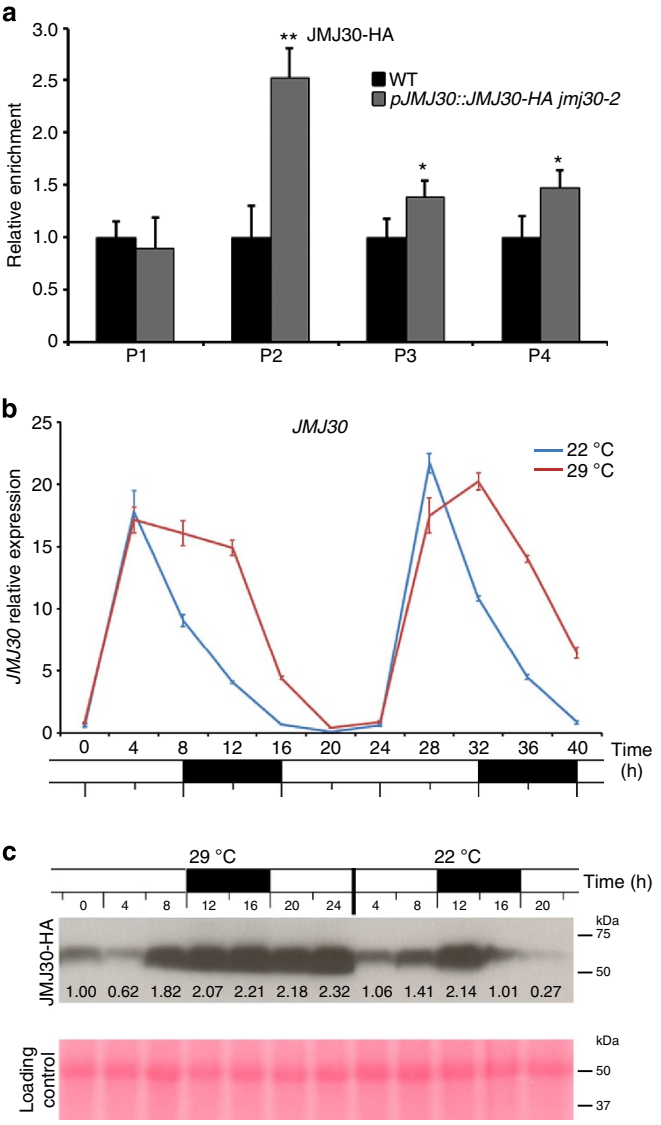

Figure 8 | Prolonged JMJ30 activity under elevated temperature directly regulates *FLC* expression. (**a**) ChIP analysis of JMJ30-HA enrichment at the *FLC* locus in 8 DAG WT and *jmj30-2 pJMJ30::JMJ30-HA* seedlings. JMJ30-HA directly binds near the transcriptional start site of the *FLC* locus. A mouse IgG was used as control. Bar indicates s.e.m. of three biological replicates; two-tailed Student's *t*-test, $*P<0.05$, $**P<0.01$. (**b**) *JMJ30* mRNA levels in WT seedlings grown under LD 22 °C and 29 °C conditions, measured over 40 h (h). Relative fold changes to 0 h are presented. Bars indicate s.d. of three biological replicates. (**c**) Relative JMJ30-HA protein levels over 24 h examined by western blot using anti-HA-HRP antibody. Total proteins from *jmj30-2 pJMJ30::JMJ30-HA* seedlings grown under LD 22 °C and 29 °C conditions were used. Ponceau Red-stained membrane is shown as a loading control. Numbers indicate relative band intensity compared with 29 °C 0 h sample. Two biological replicates were performed and one set of the data is shown here.

JMJ32 are H3K27me3 demethylases. We found that 193 of the 469 (41.15%) total downregulated genes in *jmj30 jmj32* and 213 of the 516 (41.28%) genes upregulated in *35S::JMJ30-HA* overlapped with reported H3K27me3-regulated genes (Fig. 9a, Supplementary Data 1 and 2)[33,52]. Moreover, the genes downregulated in *jmj30 jmj32* showed enrichment for PcG targets (41.15%, Fisher's exact test, P-value $= 3.499 \times 10^{-10}$) compared with the upregulated genes (201 out of 657, 30.59%, Fisher's exact test, P-value $= 0.0565$). Gene ontology analysis of the H3K27me3 targets affected by JMJ30/JMJ32 (shaded in Fig. 9a) revealed that, in terms of molecular function, genes involved in transcription factor activity (Fisher's exact test, P-value $= 8.899 \times 10^{-3}$) were more enriched, and there were slight enrichment in transcription, DNA-dependent genes in terms of biological process (Fisher's exact test, P-value $= 6.074 \times 10^{-2}$; Fig. 9b). The 40% correlation between reported H3K27me3 targets and our transcriptome profiling suggested that JMJ30/JMJ32-mediated gene regulation positively influences gene expression by demethylating the repressive H3K27me3, thereby contributing to gene de-repression.

Discussion

In this study, we revealed that the histone modifiers JMJ30 and JMJ32 demethylate H3K27me3 marks at the *FLC* locus to delay the repression of the floral repressor at elevated temperatures. In the flowering pathways, *FLC* is the central repressor that represses two floral integrators, *FT* and *SOC1*, in *Arabidopsis*[43]. We showed that JMJ30 specifically demethylates H3K27me2/3 *in vitro* (Fig. 5a,b) and *in vivo* (Supplementary Fig. 6). Moreover, *jmj30 jmj32* double mutant showed accelerated flowering when grown under 29 °C LD or SD conditions (Fig. 2c,d, Supplementary Fig. 2a,b), a temperature below the one used in basal thermotolerance experiments[53]. On the other hand, overexpression of *JMJ30-HA* led to an obvious late-flowering phenotype

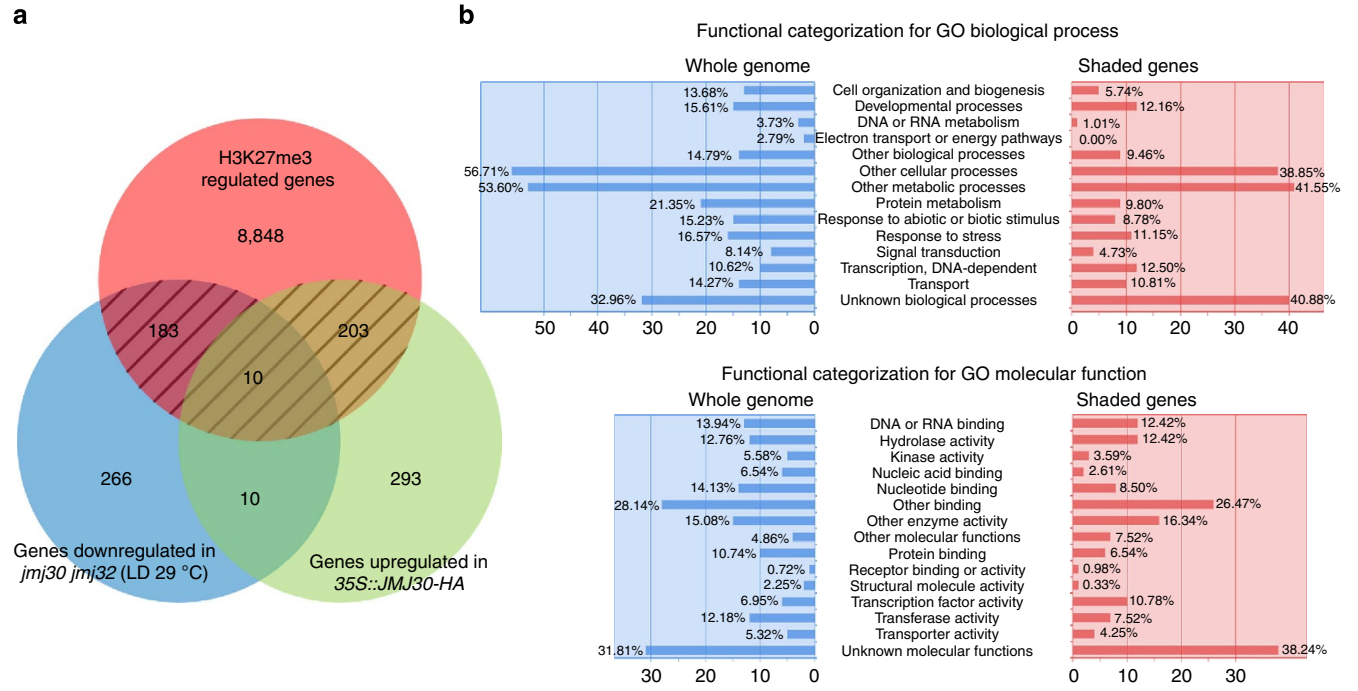

Figure 9 | Hundreds of genes are regulated by *JMJ30/JMJ32*. (**a**) Diagram showing overlap of genes downregulated in *jmj30 jmj32* grown under LD 29 °C conditions, genes upregulated in *35S::JMJ30-HA* and reported H3K27me3-regulated genes[33,52]. Genes showing a 1.5-fold change within a 90% confidence interval were considered to be differentially expressed. (**b**) Functional categorization for Gene Ontology of genes shaded in **a**.

(Supplementary Fig. 7a–d). The mutation of *fri flc* leads to early-flowering under LD (Fig. 1a,b) or SD[38] conditions with increased temperatures. Accordingly, in both *jmj30 jmj32* and *35S::JMJ30-HA* lines, we noticed that *FLC* expression was the most obviously affected (Figs 3a and 6a). The direct binding of JMJ30-HA to the transcriptional start site of the *FLC* locus shows that *FLC* is a direct target of JMJ30 (Fig. 8a; Supplementary Fig. 8). Moreover, the genetic rescue of the late-flowering phenotype of *JMJ30* overexpression by introducing the *flc* mutation strengthens the notion that JMJ30 functions through *FLC* to help regulate flowering time (Fig. 6b,c). Our work shows the importance of the balancing act between PcG-mediated histone methylation and JMJ30/JMJ32-mediated histone demethylation on H3K27 in controlling the expression of genes such as *FLC*.

Under the functional *FRI* background, *FRI jmj30 jmj32* showed only a modest decrease of *FLC* at 3-weeks-after-germination at 29 °C LD (Supplementary Fig. 10). A strong transcription activity driven by activators such as *FRI* may negatively affect the deposition of the repressive H3K27me3 marks at the *FLC* locus as previously suggested[54], possibly masking the effect of JMJ30/JMJ32. *FRI*-activated *FLC* is gradually silenced through vernalization with the accumulation of H3K27me3 (ref. 16). It would hence be interesting to study the effect of JMJ30/32 on vernalization under the *FRI* background.

JMJ30 transcript shows diurnal circadian rhythm (Fig. 8b)[41,42]. JMJ30/JMJ32-dependent *FLC* delayed repression at elevated temperatures led us to examine whether the higher activity of JMJ30 is mediated through increased expression levels or a shift in circadian rhythms. We found that *JMJ30* diurnal expression is increased by maintaining the high peak before dropping to start another cycle (Fig. 8b) and the protein is further stabilized (Fig. 8c; Supplementary Fig. 9). Although *FLC* itself is not controlled by circadian regulation, we reasoned that the increased accumulation of the JMJ30 protein at a higher temperature can help maintain the *FLC* locus in a transcriptionally permissive state. Our data showed that instability of JMJ30 protein at 22 °C is mediated by proteasomal degradation pathway, which is blocked by the proteasome inhibitor MG132 or when the plants are grown at 29 °C (Supplementary Fig. 9). Our future work includes the search for interacting partners of JMJ30 in its temperature-dependent behaviour.

Expression profiling showed that 396 out of thousands of H3K27me3-regulated genes are upregulated in *35S::JMJ30-HA* and/or downregulated in *jmj30 jmj32*. The fact that the expression profiles of many H3K27me3-regulated genes are not affected, suggests that JMJ30 and JMJ32 may only target a subset of H3K27me3-regulated genes. Because JMJ30 and JMJ32 contain only the catalytic JmjC domain, the activity of these histone modifiers may be dependent on the availability of a recruiter to the target genes. Furthermore, this JmjC domain-only group contains another member, JMJ31/AT5G19840, which has a different variant for one of its key α-KG-binding amino acids and is thus likely to be enzymatically inactive[51]. Hence, the biological function of JMJ31 remains to be elucidated.

In animals, the H3K27me3 demethylases are developmentally essential, and loss-of-function mutants of the demethylases usually lead to severe developmental defects and lethality. In mouse, JMJD3 inactivation results in perinatal lethality because of respiratory failure[55], whereas the loss of the zebrafish Utx1 leads to posterior developmental defects[56]. In *Caenorhabditis elegans*, the *utx-1* loss-of-function mutant leads to sterility and embryonic lethality[57], whereas loss of the JMJD3 homologue causes abnormal gonad development[34]. In *Arabidopsis*, one member of the KDM4/JHDM3/JMJD2 group, *REF6*, has been shown to target the floral inducer *FT*[29]. Because *FT* functions downstream of *FLC*, *ref6-1* is supposed to be epistatic to *jmj30-2 jmj32-1*, as was observed in the late-flowering phenotype of *ref6-1 jmj30-2 jmj32-1* (Supplementary Fig. 11). It is of note that the *ref6-1 jmj30-2 jmj32-1* triple mutant showed no severe developmental defects other than its late-flowering phenotype (Supplementary Fig. 11). The lack of phenotype suggests that other H3K27me3 demethylases exist in addition to these JMJ

proteins, that the feedback loop to the histone methylation is robust and flexible, or that the developmental plasticity is greater in plants than in animals.

JMJ30 and JMJ32 differ from REF6 both in their JmjC domain sequences and their lack of the JmjN domain[22]. Moreover, the JmjC domains of JMJ30, JMJ32 and REF6 showed considerable diversifications even among members of the same group, except for the highly conserved amino acids close to the Fe(II) and α-KG-binding residues[22]. Such variations within the catalytic domains of JMJ proteins have been reported in human JHDM1 and JMJD2A, both of which carry out H3K36me2 demethylation[58]. Thus, it is not uncommon for JMJ proteins with diverse variation within the JmjC domain to target the same substrate, as in the case of REF6, JMJ30 and JMJ32 in *Arabidopsis*. Crystal structures of JMJ30, JMJ32, REF6 and their cognate substrate (H3K27me3) may be helpful to verify substrate specificity-determining residues.

In addition to the floral integrators, *FT* and *SOC1*, FLC also binds and regulates many stress-responsive genes, such as the cold response genes *C-REPEAT/DRE BINDING FACTOR 1* (*CBF1*) and *CBF3* (ref. 59), and many genes involved in stress and stimulus response are implicated as target genes of JMJ30 and JMJ32 (Fig. 9b). It would be interesting to further study the roles of *JMJ30*, *JMJ32* and *FLC* in stress responses.

FLC is also known to mediate the temperature compensation mechanism of the circadian clock at elevated temperatures by lengthening the circadian period, possibly through regulating the expression of an MYB transcription factor *LUX ARRHYTHMO* (*LUX*)[60]. During circadian oscillation, the transcriptional feedback loop between the central clock genes *CIRCADIAN CLOCK ASSOCIATED 1* (*CCA1*), *LATE ELONGATED HYPOCOTYL* (*LHY*) and *TIMING OF CAB EXPRESSION 1* (*TOC1*) forms the core oscillator[61]. Two core clock genes, *CCA1* and *LHY*, directly bind and repress *JMJ30* (ref. 41), whereas JMJ30, in turn, promotes the expression of the morning-phased clock genes, *CCA1* and *LHY*[42], forming a negative feedback loop similar to the central *CCA1/LHY/TOC1* oscillation. Taken together, the interactions between *FLC*, *JMJ30* and the circadian clock genes provide a platform for crosstalk between the flowering pathway and circadian regulation to modulate plant responses to fluctuating temperatures.

One of the key players in the thermosensory pathway, the repressive H2A.Z occupancy controlling the accessibility of *PIF4*, mediates thermosensory responses by wrapping DNA more tightly at lower temperatures, thus negatively affecting *PIF4*-mediated transcription[8,9]. Although the heat-induced upregulation outcome of the H2A.Z-mediated mechanism fits the *FLC* expression profile, *FLC* does not seem to be a PIF4-regulated target gene[62]. On the other hand, recent publications showed that SVP, FLC and different splice variants of FLM form MADS-box heterocomplexes to control flowering time in response to ambient temperature changes[12–14]. The SVP-FLM-β complex delays flowering through the transcriptional repression of *FT* and *SOC1* at low temperatures, which is alleviated by the *FLM*-δ dominant-negative form at increased temperatures[13,14]. SVP may also form a complex with FLC to repress flowering at elevated temperatures, although this is less likely because SVP is rapidly degraded at elevated temperatures[13]. Taken together, our work suggests that JMJ30- and JMJ32-regulated *FLC* expression, in parallel with temperature-responsive H2A.Z nucleosome occupancy[9] and SVP-FLM cold-sensing pathways[13,14], may function to balance and coordinate flowering time in response to fluctuating temperatures.

A recent study showed that flowering in chrysanthemum is repressed at elevated temperatures through the downregulation of one of its floral inducers, *FLOWERING LOCUS T-like 3* (*FTL3*)[63]. Together with our results, this finding suggests that the need for a thermosensory balancing mechanism that represses flowering at elevated temperatures may be conserved, although the molecules involved in the process may differ. When plants are grown in an environment with fluctuating temperatures, the interplay between floral inductive and repressive signals plays a key role in determining the optimal flowering time for reproductive success. All in all, this study provides insights into the regulation of flowering time through *FLC* heat-inductive expression, which is partly achieved through the activity of H3K27 demethylases, JMJ30 and JMJ32.

Methods

Plant materials and growth conditions. All *Arabidopsis thaliana* plants used were in the background of the ecotype Columbia (Col). The *jmj32-1* (SALK_003313) allele was isolated from the SALK collections from ABRC. The alleles of *jmj30-1* (SAIL_811_H12)[41,42], *jmj30-2* (GK-454C10)[41,42] and *flc-3*[36] were described previously. Plants were grown in LDs (16-h light/8-h dark) or SDs (8-h light/16-h dark) at 22 °C or 29 °C. Genotyping primer sequences are shown in Supplementary Table 1. Total primary rosette leaves before bolting were counted to measure flowering time. Statistical analysis was performed using two-tailed Student's *t*-test.

Plasmid construction and plant transformation. To construct the *35S::JMJ30-HA* plasmid, the full-length *JMJ30* coding sequence was amplified by primer set XhoI-JMJ30_F and Bsp120I-JMJ30_R (Supplementary Table 2) and cloned into vectors pGREEN-35S-HA[64] using *Xho*I and *Bsp*120I restriction enzymes. Mutagenesis using the primers JMJ30-H326A-F and JMJ30-H326A-R produced the *35S::JMJ30H326A-HA* plasmid. The *35S::JMJ32-HA* plasmid was constructed similarly, using primer set XhoI-JMJ32_F and Bsp120I-JMJ32_R (Supplementary Table 2), and *35S::JMJ32H174A-HA* was constructed through mutagenesis using primers JMJ32-H174A-F and JMJ32-H174A-R.

For the *pJMJ30::JMJ30-GUS* and *pJMJ30::JMJ30-HA* plasmids, a 6.1-kb *JMJ30* genomic fragment (from −2,313 to +3,798; A of the start codon was set as +1) was cloned into pCR8 TOPO vector (Invitrogen) using primers JMJ30-FL_F and JMJ30-FL_R. An *Sfo*I restriction site was introduced in front of the *JMJ30* stop codon through mutagenesis using primers JMJ30-mut_F and JMJ30-mut_R (Supplementary Table 2). *GUS* or *HA* fragments were then inserted into the *Sfo*I site of the *pCR8-JMJ30* plasmid. Finally, *pJMJ30::JMJ30-GUS* and *pJMJ30::JMJ30-HA* in pCR8 were recombined into pEarleyGate303 and pHGW, respectively, using LR Clonase II (Invitrogen).

pJMJ32::JMJ32-GUS plasmid was constructed similarly to *pJMJ30::JMJ30-GUS*, differing only in that the 5.3-kb JMJ32 genomic fragment (from −3,215 to +2,084) was cloned using primer set JMJ32-FL_F and JMJ32-FL_R, and mutagenesis was performed using primers JMJ32-mut_F and JMJ32-mut_R (Supplementary Table 2).

Transgenic plants were generated by floral dipping with *Agrobacterium tumefaciens* (strain C58C1; with additional *pSOUP* helper plasmid for transformation of *pGREEN-35S::JMJ30-HA*)[65].

RNA extraction and expression analysis. For the tissue expression analysis of *JMJ30* and *JMJ32*, total RNA was isolated from young seedlings, rosette leaves, cauline leaves, stems and inflorescences. For the time-course flowering time gene expression analysis, samples were harvested from aerial parts of 5 DAG to 13 DAG seedlings for WT, *jmj30*, *jmj32* and *jmj30 jmj32*, and 1- to 3-week old seedlings for *FRI* and *FRI jmj30 jmj32* (collected at the end of the light photoperiod). Total RNA was extracted using the RNeasy plant mini kit (Qiagen) according to the manufacturer's instructions. 2 μg total RNA was used for reverse transcription using the Superscript III RT–PCR system (Invitrogen). RT–PCR with gene-specific primers (Supplementary Table 3) was performed using HotStarTaq DNA Polymerase (Qiagen) on a Thermocycler (Bio-Rad) for 15–25 cycles. Real-time quantitative PCR (qPCR) was performed on an ABI PRISM 7900HT sequence detection system (Applied Biosystems) using the KAPA SYBR FAST ABI Prism qPCR Master Mix (KAPA Biosystems). *Tip41-like* (AT4G34270) was used as an internal reference gene[66]. The relative expression of a gene of interest is calculated as $2^{-\Delta\Delta CT}$ [$\Delta\Delta C_T = \Delta C_T$ (experimental sample) − ΔC_T (control sample); $\Delta C_T = C_T$ (gene of interest)–C_T (*Tip41-like*)]. Statistical analysis was performed using two-tailed Student's *t*-test. The primer sequences are shown in Supplementary Table 3.

GUS staining. GUS staining was performed as previously described with slight modifications[67]. Briefly, plant tissues were fixed by incubating in ice-cold 90% acetone for 30 min and rinsed with rinsing solution (50 mM $NaPO_4$, pH 7.2, 0.5 mM $K_3Fe(CN)_6$ and 0.5 mM $K_4Fe(CN)_6$). The tissues were then stained in staining solution (50 mM $NaPO_4$, pH 7.2, 0.5 mM $K_3Fe(CN)_6$, 0.5 mM $K_4Fe(CN)_6$, 2 mM X-gluc) at 37 °C overnight. After staining, the tissues were placed in fixation

solution (50% ethanol, 5% acetic acid and 3.7% formaldehyde) at room temperature overnight and transferred to 100% ethanol the following day. For histological analysis, the tissues were mounted on slides with clearing solution (Hoyer's solution containing 30 ml water, 100 g chloral hydrate, 7.5 g gum Arabic, 5 ml glycerol) and observed under a SteREO Discovery.V12 Stereomicroscope (Zeiss) with images taken with an AxioCam ICc 3 (Zeiss).

ChIP assays. ChIP experiments were performed as previously described with minor modifications[67,68]. Briefly, total chromatin was extracted from 8 DAG seedlings (collected at the end of the light photoperiod) and immunoprecipitated using anti-HA (Santa Cruz Biotechnology, #sc-7392) and normal mouse IgG as a control (Santa Cruz Biotechnology, #sc-2025), or anti-H3K27me3 (Millipore, #07-449) and anti-H3 as a control (Abcam, #ab1791). Antibody dilutions of 1:200 were used (5 µl antibody in 1 ml of immunoprecipitation reaction). DNA fragments were recovered by phenol–chloroform extraction. qPCR with gene-specific primers (Supplementary Table 3) was performed on an ABI PRISM 7900HT sequence detection system (Applied Biosystems) using the KAPA SYBR FAST ABI Prism qPCR Master Mix (KAPA Biosystems). The results were first normalized to an internal control *Mutator-like* transposon (AT4G03870). For the histone modification ChIP, the relative enrichment was calculated by taking the ratio of DNA immunoprecipitated with anti-H3K27me3 antibody with that of anti-H3 antibody. Similarly, the ChIP relative enrichment of JMJ30-HA binding was calculated from the ratio between anti-HA antibody and normal mouse IgG immunoprecipitated DNA. Statistical analysis was performed using two-tailed Student's *t*-test.

Immunolocalization. The isolation of nuclei and *in situ* immunolocalization of chromatin proteins were performed as described with minor modifications[69]. Young leaves from *pJMJ30::JMJ30-HA* transgenic plants were fixed in ice-cold 4% formaldehyde Tris buffer for 20 min, rinsed and chopped into a fine suspension in LB01 buffer (15 mM Tris–HCl, pH 7.5, 2 mM EDTA, 0.5 mM spermine, 80 mM KCl, 20 mM NaCl, 0.1% Triton X-100). The sample suspension was air-dried on glass slides. Each slide was blocked with 1% BSA in 1 × PBS before incubating with mouse anti-HA antibody (Santa Cruz Biotechnology, #sc-7392) and later with CF555 goat anti-mouse IgG antibody (Biotium, #20030). A dilution of 1:200 is used for both primary and secondary antibodies. The slides were stained with DAPI and imaged with a Leica TCS SP5 confocal microscope (Leica).

Immunolocalization of protoplasts were performed as described[70]. Mouse anti-HA (Santa Cruz Biotechnology, #sc-7392) and rabbit anti-H3K27me3 (Millipore, #07-449) antibodies were used as primary antibodies, whereas CF555 goat anti-mouse IgG (Biotium, #20030) and CF488 goat anti-rabbit IgG antibodies (Biotium, #20012) were used as secondary antibodies. A dilution of 1:200 is used for both primary and secondary antibodies. The slides were stained with DAPI and imaged with a Leica TCS SPE confocal microscope (Leica).

***In vitro* histone demethylase assays.** Recombinant JMJ30-HA was transiently overexpressed in tobacco leaves and immunoaffinity-purified using anti-HA beads (Sigma, A2095). Histone demethylase assay was performed as previously described[25,29]. Briefly, the purified JMJ30-HA enzymes and substrate calf thymus histone (4 µg) were co-incubated in a 20-µl reaction mix (20 mM Tris–HCl, pH 7.5, 150 mM NaCl, 50 µM $Fe(NH_4)_2(SO_4)_2$, 1 mM α-KG, 2 mM ascorbate) for 4 h at 37 °C. The reaction products were analysed by western blotting using the following antibodies: anti-H3K27me3 (Millipore, #07-449), anti-H3K27me2 (Millipore, #07-452), anti-H3K27me1 (Millipore, #07-448), anti-H3K9me3 (Millipore, #07-442), anti-H3K9me2 (Millipore, #07-441), anti-H3K4me3 (Millipore, #07-473), anti-H3K4me2 (Millipore, #07-030), anti-H3K36me3 (Abcam, #ab9050), anti-H3K36me2 (Abcam, #ab9049) and anti-H3 (Abcam, #ab1791). A dilution of 1:1,000 is used for primary antibodies and 1:10,000 for secondary antibodies. Band intensity was calculated using ImageJ. Uncropped scans of western blot results are shown in Supplementary Fig. 13.

***In vivo* histone demethylase assays.** The protoplast transformation and *in vivo* histone demethylase assays were conducted as previously described[70]. Briefly, JMJ30-HA, JMJ30H326A, JMJ32-HA and JMJ32H174A were transiently overexpressed in *Arabidopsis* leaf protoplasts through polyethylene glycol (PEG)-mediated transformation. After one day, nuclei were isolated from the protoplasts and air-dried on the slide. Immunostaining was performed as described[69] by incubating each slide with mouse anti-HA (Santa Cruz Biotechnology, #sc-7392) and rabbit anti-H3K27me3 (Millipore, #07-449) antibodies, and then with CF555 goat anti-mouse IgG (Biotium, #20030) and CF488 goat anti-rabbit IgG antibodies (Biotium, #20012). A dilution of 1:200 is used for both primary and secondary antibodies. The slides were stained with DAPI and imaged with a Leica TCS SP8 confocal microscope (Leica). The intensities of at least 50 pairs of closely located JMJ-HA-transformed and non-transformed nuclei were analysed using ImageJ. Data were presented as a relative intensity of transformed/non-transformed nuclei and statistical analysis was performed using two-tailed Student's *t*-test.

Protein expression assays. Samples for the time-course JMJ30-HA protein expression experiment were harvested from aerial parts of 9 DAG *pJMJ30::JMJ30-HA* or *35S::JMJ30-HA* seedlings. The JMJ30-HA protein stability assay with CHX and MG132 was performed as described[13]. Total protein was extracted by grinding plant tissues in liquid nitrogen and resuspending in an equal volume of 2 × SDS loading buffer (4% SDS, 20% glycerol, 0.125 M Tris pH 6.8, 0.2% bromophenol blue, 200 mM β-mercaptoethanol). Protein samples were incubated at 95 °C for 10 min and then centrifuged for 10 min at 12,000 *g*. The supernatant was used for western blots using anti-HA-HRP (Santa Cruz Biotechnology, #sc-7392 HRP) using a dilution of 1:2,000. Band intensity was calculated using ImageJ. Uncropped scans of western blot results are shown in Supplementary Fig. 13.

Microarray analysis. For genome-wide expression analysis, two replicates of WT, *jmj30-2 jmj32-1* and *35S::JMJ30-HA* samples were analysed by NimbleGen 12 × 135K arrays (Roche). Total RNA was extracted from aerial parts of 13 DAG seedlings with the RNeasy plant mini kit (Qiagen), and double-stranded cDNA was synthesized using the SuperScript double-stranded cDNA synthesis kit (Invitrogen). cDNA samples were Cy3-labelled and hybridized following the manufacturer's instructions (Roche Nimblegen). Gene expression was analysed by Arraystar (DNAStar), and genes showing at least a 1.5-fold change within a 90% confidence interval were considered to be differentially expressed and were presented in Supplementary Data 1 and Supplementary Data 2. Gene enrichments with H3K27me3 target were tested with Fisher's exact test using R.

Dot blot. The specificity of the anti-histone antibodies was tested by dot blot (Supplementary Fig. 12). Different amount of biotin-labelled histone peptide are blotted onto a nitrocellulose membrane. Western blot analyses were then performed using the anti-histone antibodies: anti-H3K27me3 (Millipore, #07-449), anti-H3K4me3 (Millipore, #07-473) and anti-H3K36me3 (Abcam, #ab9050). A dilution of 1:1,000 is used for primary antibodies and 1:10,000 for secondary antibodies. The control experiment was probed using Strepavidin-HRP (Thermo Scientific Pierce, #21130) using a dilution of 1:1,000. The histone peptide used include: Biotinylated Histone H3 Peptide residues 1 – 21 (Epigentek, #R – 1004 – 100), Biotinylated Histone H3 Peptide residues 21 – 44 (Epigentek, #R – 1006 – 100), Biotinylated Trimethyl Histone H3K4 Peptide (Epigentek, #R – 1023 – 100), Biotinylated Trimethyl Histone H3K9 Peptide (Epigentek, #R – 1029 – 100), Biotinylated Trimethyl Histone H3K27 Peptide (Epigentek, #R – 1035 – 100) and Biotinylated Trimethyl Histone H3K36 Peptide (Epigentek, #R – 1050 – 100).

References

1. Kelly, A. E. & Goulden, M. L. Rapid shifts in plant distribution with recent climate change. *Proc. Natl Acad. Sci. USA* **105,** 11823–11826 (2008).
2. Samach, A. & Wigge, P. A. Ambient temperature perception in plants. *Curr. Opin. Plant Biol.* **8,** 483–486 (2005).
3. Wingler, A. Interactions between flowering and senescence regulation and the influence of low temperature in Arabidopsis and crop plants. *Ann. Appl. Biol.* **159,** 320–338 (2011).
4. He, Y. & Amasino, R. M. Role of chromatin modification in flowering-time control. *Trends Plant Sci.* **10,** 30–35 (2005).
5. Dennis, E. S. & Peacock, W. J. Epigenetic regulation of flowering. *Curr. Opin. Plant Biol.* **10,** 520–527 (2007).
6. Srikanth, A. & Schmid, M. Regulation of flowering time: all roads lead to Rome. *Cell. Mol. Life Sci.* **68,** 2013–2037 (2011).
7. Liu, C., Thong, Z. & Yu, H. Coming into bloom: the specification of floral meristems. *Development* **136,** 3379–3391 (2009).
8. Kumar, S. V. *et al.* Transcription factor PIF4 controls the thermosensory activation of flowering. *Nature* **484,** 242–245 (2012).
9. Kumar, S. V. & Wigge, P. A. H2A.Z-containing nucleosomes mediate the thermosensory response in Arabidopsis. *Cell* **140,** 136–147 (2010).
10. Blazquez, M. A., Ahn, J. H. & Weigel, D. A thermosensory pathway controlling flowering time in *Arabidopsis thaliana*. *Nat. Genet.* **33,** 168–171 (2003).
11. Lee, J. H. *et al.* Role of SVP in the control of flowering time by ambient temperature in Arabidopsis. *Genes Dev.* **21,** 397–402 (2007).
12. Gu, X. *et al.* Arabidopsis FLC clade members form flowering-repressor complexes coordinating responses to endogenous and environmental cues. *Nat. Commun.* **4,** 1947 (2013).
13. Lee, J. H. *et al.* Regulation of ambient temperature-responsive flowering by MADS-box transcription factor repressor complexes. *Science* **342,** 628–632 (2013).
14. Pose, D. *et al.* Temperature-dependent regulation of flowering by antagonistic FLM variants. *Nature* **503,** 414–417 (2013).
15. Seo, E. *et al.* Crosstalk between cold response and flowering in Arabidopsis is mediated through the flowering-time gene SOC1 and its upstream negative regulator FLC. *Plant Cell.* **21,** 3185–3197 (2009).
16. Angel, A., Song, J., Dean, C. & Howard, M. A polycomb-based switch underlying quantitative epigenetic memory. *Nature* **476,** 105–108 (2011).

17. Jiang, D., Wang, Y. & He, Y. Repression of FLOWERING LOCUS C and FLOWERING LOCUS T by the Arabidopsis polycomb repressive complex 2 components. *PLoS ONE* **3,** e3404 (2008).
18. Xu, Y. *et al.* A matrix protein silences transposons and repeats through interaction with retinoblastoma-associated proteins. *Curr. Biol.* **23,** 345–350 (2013).
19. Crevillen, P. & Dean, C. Regulation of the floral repressor gene FLC: the complexity of transcription in a chromatin context. *Curr. Opin. Plant Biol.* **14,** 38–44 (2011).
20. Jarillo, J. A., Pineiro, M., Cubas, P. & Martinez-Zapater, J. M. Chromatin remodeling in plant development. *Int. J. Dev. Biol.* **53,** 1581–1596 (2009).
21. Gan, E. S., Huang, J. & Ito, T. Functional roles of histone modification, chromatin remodeling and micrornas in arabidopsis flower development. *Int. Rev. Cell Mol. Biol.* **305,** 115–161 (2013).
22. Lu, F. *et al.* Comparative analysis of JmjC domain-containing proteins reveals the potential histone demethylases in Arabidopsis and rice. *J. Integr. Plant Biol.* **50,** 886–896 (2008).
23. Hong, E. H. *et al.* Temporal and spatial expression patterns of nine Arabidopsis genes encoding Jumonji C-domain proteins. *Mol. Cells* **27,** 481–490 (2009).
24. Inagaki, S. *et al.* Autocatalytic differentiation of epigenetic modifications within the Arabidopsis genome. *EMBO J.* **29,** 3496–3506 (2010).
25. Yang, W., Jiang, D., Jiang, J. & He, Y. A plant-specific histone H3 lysine 4 demethylase represses the floral transition in Arabidopsis. *Plant J.* **62,** 663–673 (2010).
26. Jeong, J. H. *et al.* Repression of FLOWERING LOCUS T chromatin by functionally redundant histone H3 lysine 4 demethylases in Arabidopsis. *PLoS ONE* **4,** e8033 (2009).
27. Yang, H. *et al.* A companion cell-dominant and developmentally regulated H3K4 demethylase controls flowering time in Arabidopsis via the repression of FLC expression. *PLoS Genet.* **8,** e1002664 (2012).
28. Liu, C., Lu, F., Cui, X. & Cao, X. Histone methylation in higher plants. *Annu. Rev. Plant Biol.* **61,** 395–420 (2010).
29. Lu, F. L., Cui, X., Zhang, S. B., Jenuwein, T. & Cao, X. F. Arabidopsis REF6 is a histone H3 lysine 27 demethylase. *Nat. Genet.* **43,** 715–U144 (2011).
30. Yu, X., Li, L., Guo, M., Chory, J. & Yin, Y. Modulation of brassinosteroid-regulated gene expression by Jumonji domain-containing proteins ELF6 and REF6 in Arabidopsis. *Proc. Natl Acad. Sci. USA* **105,** 7618–7623 (2008).
31. Saze, H., Shiraishi, A., Miura, A. & Kakutani, T. Control of genic DNA methylation by a jmjC domain-containing protein in *Arabidopsis thaliana*. *Science* **319,** 462–465 (2008).
32. Cho, J. N. *et al.* Control of seed germination by light-induced histone arginine demethylation activity. *Dev. Cell* **22,** 736–748 (2012).
33. Lafos, M. *et al.* Dynamic regulation of H3K27 trimethylation during Arabidopsis differentiation. *PLoS Genet.* **7,** e1002040 (2011).
34. Agger, K. *et al.* UTX and JMJD3 are histone H3K27 demethylases involved in HOX gene regulation and development. *Nature* **449,** 731–734 (2007).
35. Li, T. *et al.* Jumonji C domain protein JMJ705-mediated removal of histone H3 lysine 27 trimethylation is involved in defense-related gene activation in rice. *Plant Cell* **25,** 4725–4736 (2013).
36. Michaels, S. D. & Amasino, R. M. FLOWERING LOCUS C encodes a novel MADS domain protein that acts as a repressor of flowering. *Plant Cell* **11,** 949–956 (1999).
37. Michaels, S. D. & Amasino, R. M. Loss of FLOWERING LOCUS C activity eliminates the late-flowering phenotype of FRIGIDA and autonomous pathway mutations but not responsiveness to vernalization. *Plant Cell* **13,** 935–941 (2001).
38. Balasubramanian, S., Sureshkumar, S., Lempe, J. & Weigel, D. Potent induction of Arabidopsis thaliana flowering by elevated growth temperature. *PLoS Genet.* **2,** e106 (2006).
39. Li, D. *et al.* A repressor complex governs the integration of flowering signals in Arabidopsis. *Dev. Cell* **15,** 110–120 (2008).
40. Noh, B. *et al.* Divergent roles of a pair of homologous jumonji/zinc-finger-class transcription factor proteins in the regulation of Arabidopsis flowering time. *Plant Cell* **16,** 2601–2613 (2004).
41. Lu, S. X. *et al.* The Jumonji C domain-containing protein JMJ30 regulates period length in the Arabidopsis circadian clock. *Plant Physiol.* **155,** 906–915 (2011).
42. Jones, M. A. *et al.* Jumonji domain protein JMJD5 functions in both the plant and human circadian systems. *Proc. Natl Acad. Sci. USA* **107,** 21623–21628 (2010).
43. Searle, I. *et al.* The transcription factor FLC confers a flowering response to vernalization by repressing meristem competence and systemic signaling in Arabidopsis. *Genes Dev.* **20,** 898–912 (2006).
44. Winter, D. *et al.* An 'Electronic Fluorescent Pictograph' browser for exploring and analyzing large-scale biological data sets. *PLoS ONE* **2,** e718 (2007).
45. Bastow, R. *et al.* Vernalization requires epigenetic silencing of FLC by histone methylation. *Nature* **427,** 164–167 (2004).
46. Yoo, S. K. *et al.* CONSTANS activates SUPPRESSOR OF OVEREXPRESSION OF CONSTANS 1 through FLOWERING LOCUS T to promote flowering in Arabidopsis. *Plant Physiol.* **139,** 770–778 (2005).
47. Hepworth, S. R., Valverde, F., Ravenscroft, D., Mouradov, A. & Coupland, G. Antagonistic regulation of flowering-time gene SOC1 by CONSTANS and FLC via separate promoter motifs. *EMBO J.* **21,** 4327–4337 (2002).
48. Liu, C. *et al.* Direct interaction of AGL24 and SOC1 integrates flowering signals in Arabidopsis. *Development* **135,** 1481–1491 (2008).
49. Mathieu, O., Probst, A. V. & Paszkowski, J. Distinct regulation of histone H3 methylation at lysines 27 and 9 by CpG methylation in Arabidopsis. *EMBO J.* **24,** 2783–2791 (2005).
50. Lindroth, A. M. *et al.* Dual histone H3 methylation marks at lysines 9 and 27 required for interaction with CHROMOMETHYLASE3. *EMBO J.* **23,** 4286–4296 (2004).
51. Klose, R. J., Kallin, E. M. & Zhang, Y. JmjC-domain-containing proteins and histone demethylation. *Nat. Rev. Genet.* **7,** 715–727 (2006).
52. Zhang, X. *et al.* Whole-genome analysis of histone H3 lysine 27 trimethylation in Arabidopsis. *PLoS Biol.* **5,** e129 (2007).
53. Chen, J., Burke, J. J., Velten, J. & Xin, Z. FtsH11 protease plays a critical role in Arabidopsis thermotolerance. *Plant J.* **48,** 73–84 (2006).
54. Buzas, D. M., Robertson, M., Finnegan, E. J. & Helliwell, C. A. Transcription-dependence of histone H3 lysine 27 trimethylation at the Arabidopsis polycomb target gene FLC. *Plant J.* **65,** 872–881 (2011).
55. Burgold, T. *et al.* The H3K27 demethylase JMJD3 is required for maintenance of the embryonic respiratory neuronal network, neonatal breathing, and survival. *Cell Rep.* **2,** 1244–1258 (2012).
56. Lan, F. *et al.* A histone H3 lysine 27 demethylase regulates animal posterior development. *Nature* **449,** 689–694 (2007).
57. Vandamme, J. *et al.* The *C. elegans* H3K27 demethylase UTX-1 is essential for normal development, independent of its enzymatic activity. *PLoS Genet.* **8,** e1002647 (2012).
58. Chen, Z. *et al.* Structural insights into histone demethylation by JMJD2 family members. *Cell* **125,** 691–702 (2006).
59. Deng, W. *et al.* FLOWERING LOCUS C (FLC) regulates development pathways throughout the life cycle of Arabidopsis. *Proc. Natl Acad. Sci. USA* **108,** 6680–6685 (2011).
60. Edwards, K. D. *et al.* FLOWERING LOCUS C mediates natural variation in the high-temperature response of the Arabidopsis circadian clock. *Plant Cell* **18,** 639–650 (2006).
61. Nagel, D. H. & Kay, S. A. Complexity in the wiring and regulation of plant circadian networks. *Curr. Biol.* **22,** R648–R657 (2012).
62. Oh, E., Zhu, J. Y. & Wang, Z. Y. Interaction between BZR1 and PIF4 integrates brassinosteroid and environmental responses. *Nat. Cell Biol.* **14,** 802–809 (2012).
63. Nakano, Y., Higuchi, Y., Sumitomo, K. & Hisamatsu, T. Flowering retardation by high temperature in chrysanthemums: involvement of FLOWERING LOCUS T-like 3 gene repression. *J. Exp. Bot.* **64,** 909–920 (2013).
64. Hellens, R. P., Edwards, E. A., Leyland, N. R., Bean, S. & Mullineaux, P. M. pGreen: a versatile and flexible binary Ti vector for Agrobacterium-mediated plant transformation. *Plant Mol. Biol.* **42,** 819–832 (2000).
65. Clough, S. J. & Bent, A. F. Floral dip: a simplified method for Agrobacterium-mediated transformation of *Arabidopsis thaliana*. *Plant J.* **16,** 735–743 (1998).
66. Czechowski, T., Stitt, M., Altmann, T., Udvardi, M. K. & Scheible, W. R. Genome-wide identification and testing of superior reference genes for transcript normalization in Arabidopsis. *Plant Physiol.* **139,** 5–17 (2005).
67. Sun, B., Xu, Y., Ng, K. H. & Ito, T. A timing mechanism for stem cell maintenance and differentiation in the Arabidopsis floral meristem. *Genes Dev.* **23,** 1791–1804 (2009).
68. Ito, T., Takahashi, N., Shimura, Y. & Okada, K. A serine/threonine protein kinase gene isolated by an in vivo binding procedure using the Arabidopsis floral homeotic gene product, AGAMOUS. *Plant Cell Physiol.* **38,** 248–258 (1997).
69. Lysak, M., Fransz, P. & Schubert, I. Cytogenetic analyses of Arabidopsis. *Methods Mol. Biol. (Clifton, NJ)* **323,** 173–186 (2006).
70. Lee, M. H., Lee, Y. & Hwang, I. *In vivo* localization in Arabidopsis protoplasts and root tissue. *Methods Mol. Biol. (Clifton, NJ)* **1043,** 113–120 (2013).

Acknowledgements

We thank H. Yu for generously providing *flc-3* seeds, Y. Tamada and D. Buzas for their critical comments and discussions on this work, and *Arabidopsis* Biological Resource Center for providing the T-DNA insertion line of *JMJ30* and *JM32*. This work was supported by research grants to T.I. from Temasek Life Sciences Laboratory (TLL), the National Research Foundation, Prime Minister's Office, Singapore, under its Competitive Research Program (CRP Award No. NRF-CRP001-108) and PRESTO, Japan Science and Technology Agency, 4-1-8 Honcho Kawaguchi, Saitama, Japan. The funders had no role in study design, data collection and analysis, decision to publish, or preparation of the manuscript.

Author contributions

T.I. conceived the research. E.-S.G., T.I. and Y.X. designed the experiments. E.-S.G., J.-Y.W. and J.G.G. performed the experiments. W.-Y.W. participated in the confocal imaging. B.S. and J.H. participated in the ChIP assays. E.-S.G., Y.X. and T.I. wrote the paper. All authors discussed the results and made substantial contributions to the manuscript.

Additional information

Accession codes: The NimbleGen 12 × 135 K expression array data sets are deposited in the NCBI Gene Expression Omnibus (GEO) under the accession code GSE51898.

Supplementary Information accompanies this paper at http://www.nature.com/naturecommunications

Competing financial interests: The authors declare no competing financial interests.

Reprints and permission information is available online at http://npg.nature.com/reprintsandpermissions/

How to cite this article: Gan, E.-S. *et al.* Jumonji demethylases moderate precocious flowering at elevated temperature via regulation of *FLC* in *Arabidopsis*. *Nat. Commun.* 5:5098 doi: 10.1038/ncomms6098 (2014).